

# RSC Advances

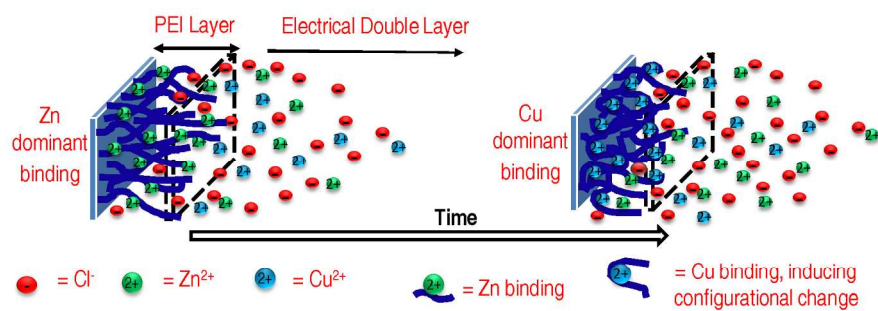


This is an *Accepted Manuscript*, which has been through the Royal Society of Chemistry peer review process and has been accepted for publication.

*Accepted Manuscripts* are published online shortly after acceptance, before technical editing, formatting and proof reading. Using this free service, authors can make their results available to the community, in citable form, before we publish the edited article. This *Accepted Manuscript* will be replaced by the edited, formatted and paginated article as soon as this is available.

You can find more information about *Accepted Manuscripts* in the [Information for Authors](#).

Please note that technical editing may introduce minor changes to the text and/or graphics, which may alter content. The journal's standard [Terms & Conditions](#) and the [Ethical guidelines](#) still apply. In no event shall the Royal Society of Chemistry be held responsible for any errors or omissions in this *Accepted Manuscript* or any consequences arising from the use of any information it contains.



254x190mm (200 x 200 DPI)

# Mathematically modelling competitive ion absorption in a polymer matrix<sup>†</sup>

Stanley J. Miklavcic,<sup>\*a,b</sup> Magnus Nydén,<sup>c</sup> Johan B. Lindén<sup>c</sup> and Jordan Schulz<sup>a</sup>

Received Xth XXXXXXXXXXXX 20XX, Accepted Xth XXXXXXXXXXXX 20XX

First published on the web Xth XXXXXXXXXXXX 20XX

DOI: 10.1039/b000000x

A recent publication [Lindén *et al.*, *R.S.C. Advances*, 2014, **4**, 25063-25066] describing a material with extreme efficiency and selectivity for adsorbing copper opens up the possibility of large scale purification technologies and new materials for prevention of biological growth, both in bulk and on surfaces. On the molecular scale, the material's efficiency and selectivity depends on competitive metal ion diffusion into a nanometer thin polymer film and on competitive binding of metal ions to specific ligand sites. We present and explore two reaction-diffusion models describing the detailed transport and competitive absorption of metal ions in the polymer matrix by studied in [Lindén *et al.*, *R.S.C. Advances*, 2014, **4**, 25063-25066]. The diffusive transport of the ions into an interactive, porous polymer layer of finite thickness, supported by an impermeable substrate and in contact with an infinite electrolyte reservoir, is governed by forced diffusion equations, while metal ion binding is modelled by a set of coupled reaction equations. The qualitative behavior observed in experiments can be reproduced and explained in terms of a combination of (a) differing ion diffusive rates and, effectively, (b) an ion exchange process that is superimposed on independent binding processes. The latter's origin is due to conformational changes taking place in the polymer structure in response to the binding of one of the species. The results of simulations under a diverse set of parameter conditions are discussed in relation to experimental observations.

## 1 Introduction

Water contaminated with toxic metal ions are often a result of industrial processes<sup>2</sup> but also through antifouling paints leaching metal-based biocides<sup>3,4</sup>. Increased awareness of the toxic effects and economic aspects of reuse of water, sludge and sediment and recovery of metal waste are driving forces for research in new and improved metal-removal technologies<sup>2,5</sup>. A wide range of techniques have been studied over past decades including chemical precipitation, ion-exchange, adsorption, membrane filtration, coagulation-flocculation, flotation and electrochemical methods<sup>6</sup>.

Adsorption and ion-exchange technologies have proven to be effective methods for the removal of various metals from aqueous solutions<sup>6,7</sup>. In both methods a selectivity for specific metal ions is attributed to functional groups on either the natural or chemically modified surface of the material<sup>6-8</sup>.

The separation process of the metal ions from the aque-

ous phase is typically described as adsorption onto the surface of the solid phase of either the adsorbent<sup>9</sup> or the ion-exchange resin<sup>2</sup>. Wan Ngah, et al.<sup>9</sup> evaluated the adsorption capacities and rates of Cu(II) ions onto chitosan and chitosan blended with poly(vinyl alcohol) (PVA). They found that the Langmuir model correlated well with the adsorption isothermal data and that the kinetic experimental data correlated well with the second-order kinetic model which would indicate the rate-limiting step as chemical sorption. Beatty, et al.<sup>2</sup> also analysed the performance of their ion-exchange resin using a Langmuir isotherm and second-order kinetic model. They described their slower rate of adsorption in comparison to a commercially available resin as being dependant on a longer ion diffusion path into the polymer layer on the silica support material.

Although adsorption isotherms such as the Langmuir play an important role in the search for an ideal metal ion adsorbent, they might face limitations when the metal ion uptake is not solely adsorption<sup>10</sup>. In one study of chitosan and its glutaraldehyde cross-linked derivative it was concluded that the metal ion uptake mechanism was absorption within the polymers rather than adsorption on the polymer surface<sup>11</sup>. This indicates the importance of investigating the possibility of considering the metal ion uptake of a pure polymer sorbent or polymer modified sorbent as an absorption process. Furthermore the effect of conformational changes within polymers

<sup>†</sup> Electronic Supplementary Information (ESI) available: [details of any supplementary information available should be included here]. See DOI: 10.1039/b000000x/

<sup>a</sup> Phenomics and Bioinformatics Research Centre, University of South Australia, Mawson Lakes, SA 5095, Australia. Fax: +61 8 830 25785; Tel: +61 8 830 23788; E-mail: stan.miklavcic@unisa.edu.au

<sup>b</sup> Australian Centre for Plant Functional Genomics, Hartley Grove, Urrbrae, SA 5064, Australia.

<sup>c</sup> Ian Wark Research Institute, University of South Australia, Mawson Lakes, SA 5095, Australia.

could also play an important role in the metal uptake mechanism<sup>12,13</sup>.

We address the following problem: to model the temporal and spatial development of competitive absorption of metal ions within a polymer matrix. The example system we have in mind to model is a polyethyleneimine (PEI) layer adsorbed onto an impermeable planar surface and exposed to a bulk electrolyte mixture. Recently, Lindén and coworkers<sup>1</sup> experimented with a surface-bound, cross-linked PEI layer exposed to either an artificial sea water solution or actual sea water. They found that the PEI layer exhibited preferential absorption for certain metal cations, namely copper ( $\text{Cu}^{2+}$ ), zinc ( $\text{Zn}^{2+}$ ) and cadmium ( $\text{Cd}^{2+}$ ), in that order of preference. The competitive absorption of metal ions into the PEI layer was performed at equimolar concentration of about  $3 \mu\text{M}$ <sup>1</sup>, which is roughly 200 times higher than the levels at which the ions are present in sea water<sup>14,15</sup>. However, this concentration is considerably lower than employed in other metal ion uptake studies involving PEI<sup>2,5,16–18</sup>.

Linden has recently shown that polyethyleneimine (PEI) is extremely effective and selective to copper in salt- and fresh water and that it self-adsorbs into a thin film on porous silica particles (reference to full paper in the same journal). The latter allows for very large surface area exposure. Furthermore, the cross-linked polymer is mechanically and chemically stable in a wide pH range. Taken together, the material properties of PEI and silica porous silica particles allows for large scale technologies for purifying water from copper as well as preventing biological growth at surfaces and in bulk. Given the need for copper purification and the large scale potential of PEI/silica particle system we aim to increase our understanding of the molecular-scale processes by addressing the following problem in more detail: to model the temporal and spatial development of competitive absorption and chemical binding of metal ions within a polymer matrix.

That PEI can take up metal ions through chemical binding is known<sup>19–21</sup>. Rivas, et al.<sup>20</sup>, working with PEI tetramers (TETA) in solution showed that the TETA molecules could take up copper and Kobayashi with coworkers in Ref.<sup>19</sup>, who also worked in solution, found that the branched structure of PEI gave a more favourable complexation than the linear structure. Metal ion uptake studies have also been reported for cases where PEI was attached to the surface of a support material<sup>2,5,16–18</sup>. However, what was not explored prior to the work of Lindén, et al.<sup>1</sup> was the competitive absorption behavior of PEI in the presence of a solution mixture, the predominant results of which are shown in Figure 1. In particular, Lindén, et al.<sup>1</sup> found that the cross-linked PEI matrix displayed anomalous preference for copper in the following sense. At a very early stage post exposure, zinc ions, and to a lesser extent cadmium ions, were rapidly absorbed forming complexes with specific sites in the matrix. Later, increasing amounts of cop-

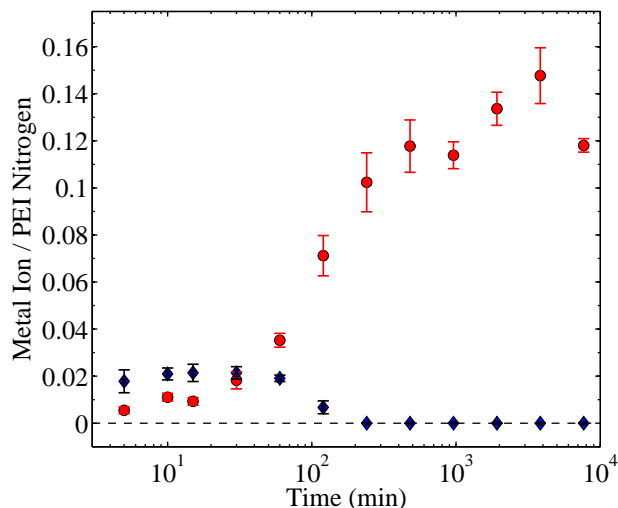


**Fig. 1** Graph showing metal ion uptake over time in terms of a metal ion to (PEI) nitrogen ratio as a function of time after immersion in artificial seawater (pH 8). Blue diamonds denote Zn/N ratios, while red circles denote Cu/N ratios. In this experiment 12 different metal ions were present at the same time:  $\text{Al}^{3+}$ ,  $\text{Cd}^{2+}$ ,  $\text{Co}^{2+}$ ,  $\text{Cr}^{3+}$ ,  $\text{Cu}^{2+}$ ,  $\text{Fe}^{2+}$ ,  $\text{Mn}^{2+}$ ,  $\text{Mo}^{6+}$ ,  $\text{Ni}^{2+}$ ,  $\text{Pb}^{2+}$ ,  $\text{V}^{3+}$ ,  $\text{Zn}^{2+}$ :  $[\text{Me}^{n+}] = 3 \mu\text{M}$  ( $[\text{Cu}^{2+}] = 200 \text{ ppb}$ ). Data shown in this figure was adapted from Ref.<sup>1</sup>

per complexes were detected. However, rather than each metal ion complex increasing in number monotonically with prolonged exposure to a bulk electrolyte reservoir, it was found that the copper ion complexes increased significantly, reaching a steady state plateau value, while the zinc and cadmium complexes reached a maximum amount and then decreased to levels below instrument sensitivity. Effectively, the quantities of bound zinc and cadmium approached zero at steady state. It is this entire time series of phenomena that we seek to address in this paper. Reasons for the findings were postulated as were the possible applications of the phenomena, such as the extraction of minerals from seawater (specifically, the extraction of copper from the oceans), the refinement and purification of industry waste water as well as the more community-based treatment of recycled water<sup>1</sup>.

In explanation for the two phases of uptake, Lindén, et al.<sup>1</sup> stated that “the binding kinetics were faster for zinc but with copper binding being thermodynamically favored”. On the face of it, this would seem a natural conclusion to draw. However, the physical system proves to be more complex. In this paper we present and investigate quantitatively two alternate scenarios which explain the competitive behavior at least qualitatively. In the first scenario we postulate that the differential binding phenomenon is simply *not* due to faster binding kinetics on the part of  $\text{Zn}^{2+}$  and a steady state or thermodynamic

preference toward  $\text{Cu}^{2+}$  binding, but rather to a difference in diffusive properties of the two ions *in conjunction with an ion exchange reaction*. In the second scenario, in recognition of the findings of Nurchi, et al.<sup>13</sup>, who argued that the binding of  $\text{Cu}^{2+}$  induces a conformational change in the matrix structure, we postulate that the competitive binding phenomenon is due to a *conjunction* of differential diffusion and a *conformational change* upon  $\text{Cu}^{2+}$  binding that both precludes the binding of  $\text{Zn}^{2+}$  ions as well as ejects already bound  $\text{Zn}^{2+}$  in the neighborhood of the copper binding site.

Although the (two) models we introduce and explore below target the aforementioned experimental system directly, it is not unreasonable to anticipate that the models and the simulation results derived from them, have applicability in other contexts, notably in biology. Dealing, for instance, in ion specific membrane transport<sup>22</sup>.

The remainder of this paper is organized as follows. In Section 2 we describe the two scenarios hypothesized to explain the findings as well as introduce other essential particulars of the models. In Section 3 the mathematical descriptions of the physical models are outlined. Here, the key model parameters are introduced. In that section we also outline the numerical solution method followed. Section 4 presents some illustrative example simulations, which explore the important regions of parameter space. We summarize our findings and provide concluding remarks in Section 5.

## 2 Polymer matrix geometry & kinetic transport mechanisms

In line with the experimental system, we adopt the model of a thin, charged polymer matrix of thickness  $D$  that has been adsorbed to an uncharged, solid and impermeable substrate. We assume in the following that  $D$  remains a constant and is not responsive to ion uptake (an alternate model approach showing this effect can be found in<sup>23,24</sup>). We further assume the polymer matrix to be homogeneous and uniformly porous. Moreover, it is homogeneously permeable to mobile ions. We assume the matrix to possess a constant (total) density of binding sites,  $n_{PEI_{tot}}$ , which are either equally accessible to both binding cations (Scenario I) or are equally divided into a number that are accessible to only  $\text{Cu}^{2+}$  ( $n_{PEI_{1,tot}}$ ) or only  $\text{Zn}^{2+}$  ( $n_{PEI_{2,tot}}$ ) (Scenario II). In either case, the binding sites are assumed to be negatively charged with unit valence ( $z_{PEI} = z_{PEI_1} = z_{PEI_2} = -1$ ). The adsorbed layer is in contact with a 2:1 mixed bulk electrolyte comprising  $\text{Cu}^{2+}$ ,  $\text{Zn}^{2+}$ ,  $\text{Cl}^-$  ions.

The important processes taking place in this problem include mobile ion diffusion into or out from the polymer matrix, with ions sourced from the electrical double layer adjacent to the polymer matrix. In addition, there are two fundamental chemical binding reactions, one for each of the cations

$\text{Cu}^{2+}$  and  $\text{Zn}^{2+}$  and their respective binding sites within the matrix. The details of these intrinsic reactions are given in the next section. In Section 4 we show that these effects alone are *insufficient* to explain the experimental observations. Therefore, in addition to the core binding reactions we invoke a secondary reaction mechanism, which will be explained in Section 3 via two model formulations, that completes the picture and quite convincingly accounts for observed phenomenon. Finally, the outcome of all the binding events (as well as the underlying charged state of the matrix) result in an inhomogeneous distribution of charge that establishes an inhomogeneous electric potential field. The field gradient in turn influences the rate of influx of ions (indeed it influences which ions enter the matrix as well as their diffusion rates).

With respect to the electric field, we envisage that the mobile ions external to the matrix diffuse sufficiently fast that the ionic double layer outside the matrix is always in a state of quasi equilibrium. That is, the ions are sufficiently responsive on the time scale of the processes taking place within the layer that the double layer adjusts immediately in response to changes in the state of polymer charge. At the low values of accumulated charge and low bulk electrolyte concentrations considered, we assume that the electrical double layer outside the matrix is adequately described by the Poisson-Boltzmann model<sup>25,26</sup>. We remark that although we will associate differences in ion diffusivities with differences in effective ionic radii (see Section 4), our models do not include any explicit ion size effects, which not only could influence the double layer structure adjacent to the polymer layer at high concentrations<sup>27</sup> but would likely play an influential role in shifting the balance in the competition for absorption sites even at low electrolyte concentrations. We envisage the latter effect to be akin to the site exclusion phenomenon simulated in the hydrated ion model of competitive ion adsorption<sup>28</sup>. We reserve for the future the task of considering this effect, whose significance is comparable to and indeed warrants a more accurate description of the polymer structure itself, which is presently unavailable.

## 3 Governing equations

The charge distribution within the polymer matrix comprises free ions, here denoted by the index  $i = 1, \dots, n$  and bound charges, here denoted by the index  $j = 1, \dots, m$ . As our focus is on the competitive binding of  $\text{Cu}^{2+}$  and  $\text{Zn}^{2+}$  in a polymer matrix, we restrict attention to determining the distribution of these two ions plus that of a common counterion,  $\text{Cl}^-$ . Thus,  $n = 3$ . In this same context, the bound species are  $\text{PEI}^-$ ,  $\text{CuPEI}^+$  and  $\text{ZnPEI}^+$ , as explained below. Thus,  $m = 3$  or 4,



as explained below. The charge density is given as,

$$\rho(x;t) = \sum_{i=1}^n z_i e n_i(x;t) + \sum_{j=1}^m z_j e n_j(x;t), \quad (1)$$

where  $n_i$  and  $n_j$  refer to the number densities of the respective species,  $i$  and  $j$  at position  $x$  at time  $t$ , with  $z_i$  and  $z_j$  being their respective valencies;  $e$  is the electronic charge.

### 3.1 Competitive binding scenario I: Ion exchange model

To describe the competitive absorption of Cu and Zn ions we model the ion binding event here assuming a single type of binding site, denoted  $PEI^-$ . In this case we first identify two binding reactions, one for each of the ions. These reactions involve a mix of free ions and bound charge sites:



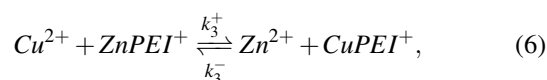
Thus far, these reactions take place explicitly independent of each other and occur at different rates given by

$$r_1 = \frac{\partial[CuPEI^+]}{\partial t} = k_1^+[Cu^{2+}][PEI^-] - k_1^-[CuPEI^+], \quad (4)$$

$$r_2 = \frac{\partial[ZnPEI^+]}{\partial t} = k_2^+[Zn^{2+}][PEI^-] - k_2^-[ZnPEI^+], \quad (5)$$

where we have denoted the molar concentration of component  $X$  by the symbol  $[X]$  (M); molar concentrations are related to number densities ( $\text{cm}^{-3}$ ) by the relation,  $n_X = N_A 10^{-3}[X]$ , where  $N_A$  is Avogadro's number,  $6.022 \times 10^{23} \text{ mol}^{-1}$ . The rate constants of forward (+) and reverse (-) reactions are denoted by the parameters  $k^\pm$ .

In addition to these binding reactions we include in this scenario the following exchange reaction,



which occurs at the rate

$$r_3 = k_3^+[Cu^{2+}][ZnPEI^+] - k_3^-[Zn^{2+}][CuPEI^+]. \quad (7)$$

The rates,  $r_1$  and  $r_2$ , describe the rates of production of  $CuPEI^+$  and  $ZnPEI^+$ , respectively, as well as the consumption of  $Cu^{2+}$  and  $Zn^{2+}$ , the latter being the free mobile ions. Given the additional exchange reaction, the rate equations 4 and 5 must be supplemented by the effect of the exchange rate

$r_3$ :

$$\begin{aligned} \frac{\partial[CuPEI^+]}{\partial t} = & \underbrace{k_1^+[Cu^{2+}][PEI^-]}_{\text{association}} - \underbrace{k_1^-[CuPEI^+]}_{\text{dissociation}} \\ & + \underbrace{k_3^+[Cu^{2+}][ZnPEI^+]}_{\text{exchange (forward)}} - \underbrace{k_3^-[Zn^{2+}][CuPEI^+]}_{\text{exchange (backward)}}, \end{aligned} \quad (8)$$

and, similarly,

$$\begin{aligned} \frac{\partial[ZnPEI^+]}{\partial t} = & \underbrace{k_2^+[Zn^{2+}][PEI^-]}_{\text{association}} - \underbrace{k_2^-[ZnPEI^+]}_{\text{dissociation}} \\ & + \underbrace{k_3^-[Zn^{2+}][CuPEI^+]}_{\text{exchange (forward)}} - \underbrace{k_3^+[Cu^{2+}][ZnPEI^+]}_{\text{exchange (backward)}}. \end{aligned} \quad (9)$$

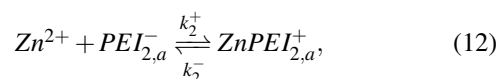
These equations are explicit, ordinary differential equations in time but are implicitly also functions of position  $x$  through the dependencies of the respective concentrations on position. That is, these equations must be solved locally (at  $x$ ) throughout the polymer matrix.

This binding model must satisfy the conservation condition that the total number of sites remains fixed irrespective of whether there is binding or not. The relevant equation is

$$n_{PEI_{tot}} = N_A 10^{-3} [[PEI^-] + [CuPEI^+] + [ZnPEI^+]] = \text{constant}. \quad (10)$$

### 3.2 Competitive binding scenario II: Polymer relaxation model

We formulate this model situation by assuming, at least initially, that there are two types of binding sites (labelled with subscripts 1 and 2), one for each of the divalent metal ions,  $Cu^{2+}$  and  $Zn^{2+}$ . In addition to the standard binding reaction equations we presume here that site type 2 can exist in one of two binding states, an active binding state, labelled  $\{2, a\}$ , and an inactive binding state, labelled  $\{2, ia\}$ . The fundamental reaction equations are then slightly modified versions of eq 2 and 3,



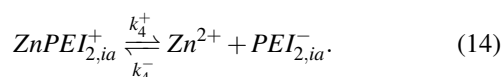
where, apart from the numerical subscripts there now appears in eq 12 the reference  $\{2, a\}$  as a reminder that the chemical reaction takes place on an active type-2 binding site only.

A point of major differentiation between this scenario and that of Scenario I is the assumption that the binding of  $Cu^{2+}$  to its specific binding site induces a local conformational change

in the polymer matrix which converts an active type-2 binding site to its inactive binding state. This conversion, which may be structural or chemical, either prevents the binding of  $Zn^{2+}$  to its specific binding site or induces an unbinding of an existing bound  $Zn^{2+}$ . For the latter possibility, we imagine the two-step reaction process



followed by a  $Zn^{2+}$  unbinding or dissociation reaction



Once in the inactive state, the forward reaction in eq 14 is considered to be sufficiently rapid as to be a spontaneous event. Hence, one would expect  $k_4^+ \gg k_4^-$ . Indeed, assuming the limiting case of complete forward reaction, we can summarize eq 13 and 14 in one reaction equation,



The rate of production of free  $Zn^{2+}$  (assuming complete dissociation) is then governed by the rate at which reaction 15 proceeds, which is given by

$$r_3 = [CuPEI_1^+] \left( \underbrace{k_3^+ [ZnPEI_{2,a}^+]}_{\text{inactivation}} - \underbrace{k_3^- [Zn^{2+}][PEI_{2,ia}^-]}_{\text{rapid dissociation}} \right), \quad (16)$$

which is also the rate at which  $ZnPEI_{2,a}^+$  is converted to  $PEI_{2,ia}^-$ . To be completely consistent in our reasoning we should actually not consider the possibility of a reverse reaction in eq 16. That is, we should set  $k_3^- \equiv 0$  from the outset. Nevertheless, we include the reverse terms in eq 15 and 16 for formal completeness only and point out that in our calculations we avoid adopting significant values of  $k_3^-$  or  $k_4^-$  and so maintain the forward balance of the reactions.

As for the case of converting the state of a vacant type-2 binding site, we invoke the model reaction



which occurs at the rate

$$r_5 = [CuPEI_1^+] \left( \underbrace{k_5^+ [PEI_{2,a}^-]}_{\text{inactivation}} - \underbrace{k_5^- [PEI_{2,ia}^-]}_{\text{activation}} \right). \quad (18)$$

In all probability, the latter rate constants should satisfy the inequality  $k_5^+ \gg k_5^-$ , implying that the reverse reaction all but never takes place. Note also that based on our intuitive understanding of the conformational change process we expect the  $k_5^+$  value to be different, but perhaps not significantly different, from the  $k_3^+$  value.

As in the case of the single site binding model, this two-site binding model must satisfy conservation conditions: the total number of sites remains fixed irrespective of whether there is binding or not. The relevant equations are

$$n_{PEI_{1,tot}} = N_A 10^{-3} [PEI_1^-] + [CuPEI_1^+] = \text{constant}, \quad (19)$$

$$n_{PEI_{2,tot}} = N_A 10^{-3} [PEI_{2,ia}^-] + [PEI_{2,a}^-] + [ZnPEI_{2,a}^+] + [ZnPEI_{2,ia}^+] = \text{constant}. \quad (20)$$

**Remark:** It is important to point out that Scenario I and II are different in two major respects. Firstly, Scenario I describes a process of physical *exchange* of  $Cu^{2+}$  for  $Zn^{2+}$ , with no alteration of the polymer matrix, while Scenario II describes a *conformational reaction* within the polymer resulting from the binding of  $Cu^{2+}$ . These are quite distinct phenomena. The second point of differentiation is that Scenario I assumes a common type of binding site, equally accessible to both  $Zn^{2+}$  and  $Cu^{2+}$ , while Scenario II assumes specific sites for the respective ions. It is not difficult to imagine other scenarios that are intermediate or hybrids of the two cases. However, it is not the purpose of this paper to establish which of these is most applicable to the given experimental system. Our purpose is only to demonstrate that an additional interaction involving the ions (such as described by Scenarios I and II) is necessary to produce behavior reminiscent of the experiments.

### 3.3 Ion diffusion

The intrusion of ions into the polymer matrix is assumed to take place by means of (forced) diffusion. Exposure of the matrix to an electrolyte solution with ions at a finite bulk concentration and thus larger chemical potential induces the transport of ions into the polymer layer. The process is largely driven by concentration gradients but also by an electric field gradient arising from the inhomogeneous charge distribution. Three ions are assumed sufficiently mobile to diffuse into the matrix:  $Cu^{2+}$ ,  $Zn^{2+}$  and  $Cl^-$ . The rates at which ions diffuse into the matrix are here governed by their intrinsic diffusion constants and their respective ionic conductivities. However, it is well known that diffusion of dissolved molecules is reduced, relative to bulk diffusion, by polymer chains through several mechanisms<sup>29</sup>. While it is necessary for a quantitative evaluation with experiments to consider these effects, for the present task of illustrating qualitative behavior and in the absence of detailed quantitative experimental information about

the present system, we shall assume, unless otherwise stated, that the values of the ion diffusion parameters are equal to their bulk values<sup>30</sup>. The equations governing forced ion diffusion are

$$\begin{cases} \frac{\partial[Cu^{2+}]}{\partial t} = D_{Cu} \frac{\partial^2[Cu^{2+}]}{\partial x^2} - \frac{ez_{Cu}}{\lambda_{Cu}} \frac{\partial}{\partial x} \left[ [Cu^{2+}] \frac{\partial \psi}{\partial x} \right] - P_{Cu}, \\ \frac{\partial[Zn^{2+}]}{\partial t} = D_{Zn} \frac{\partial^2[Zn^{2+}]}{\partial x^2} - \frac{ez_{Zn}}{\lambda_{Zn}} \frac{\partial}{\partial x} \left[ [Zn^{2+}] \frac{\partial \psi}{\partial x} \right] - P_{Zn}, \\ \frac{\partial[Cl^-]}{\partial t} = D_{Cl} \frac{\partial^2[Cl^-]}{\partial x^2} - \frac{ez_{Cl}}{\lambda_{Cl}} \frac{\partial}{\partial x} \left[ [Cl^-] \frac{\partial \psi}{\partial x} \right], \end{cases} \quad 0 < x < D, \quad t > 0, \quad (21)$$

where the terms on the left hand sides of the respective equations combined with the first terms on the right hand sides conjointly comprise the usual free diffusion equations for the mobile ions,  $Cu^{2+}$ ,  $Zn^{2+}$  and  $Cl^-$ . The second terms on the right hand sides represent the leading order, nonideal activity, contributions to the gradient of the chemical potentials. In the mean-field model these contributions involve the gradient of the self-consistent mean-field electric potential. The final terms on the right hand sides of the equations for  $Cu^{2+}$  and  $Zn^{2+}$  refer to the net consumption/production of these ions as determined by their respective sets of chemical absorption reactions. Absorption of the ions means they are no longer free to participate in the diffusive process. The effects, represented by the functions  $P_{Cu}$  and  $P_{Zn}$  are therefore treated as that of sinks. The opposite is true of ions produced through the reaction events. The latter effects are treated as that of sources. In eq 21, the  $\lambda_i$  parameters are ionic drag coefficients, while the  $D_i$  parameters are ion diffusion constants.

Equations 21 are complemented by boundary and initial conditions. Initially, we suppose there are no mobile ions present. Thus,

$$[X](x;0) = 0, \quad X = \{Cu^{2+}, Zn^{2+}, Cl^-\}, \quad 0 \leq x \leq D, \quad t = 0. \quad (22)$$

At  $x = 0$  we suppose there is no flux of ions through the substrate

$$\frac{\partial[X]}{\partial x}(0;t) = 0, \quad X = \{Cu^{2+}, Zn^{2+}, Cl^-\}, \quad x = 0, \quad t \geq 0, \quad (23)$$

while at  $x = D$  we suppose there is a ready supply of mobile ions equal to the concentration of ions in the double layer adjacent to the polymer interface,

$$[X](D^-;t) = [X](D^+;t) \equiv \frac{n_X^\infty}{N_A 10^{-3}} \exp(-ez_X \psi(D^+;t)/kT), \quad X = \{Cu^{2+}, Zn^{2+}, Cl^-\}, \quad x = D, \quad t \geq 0. \quad (24)$$

### 3.4 Electric potential

Given that the bound ions are also charged contributions, the concentrations will also need to be incorporated into the ex-

pression for the charge density. The explicit expression for the charge density is

$$\begin{aligned} \rho(x;t) &= \sum_{i=1}^n z_i e n_i(x;t) + \sum_{j=1}^m z_j e n_j(x;t) \\ &= e N_A 10^{-3} \{ z_{Cu} [Cu^{2+}](x;t) + z_{Zn} [Zn^{2+}](x;t) + z_{Cl} [Cl^-](x;t) \} \\ &\quad + e N_A 10^{-3} \{ z_{PEI} [PEI^-](x;t) + z_{CuPEI} [CuPEI^+](x;t) \\ &\quad + z_{ZnPEI} [ZnPEI^+](x;t) \}. \end{aligned} \quad (25)$$

The nonuniform charge content of the polymer layer generates an electric field which influences both the rate and extent of ion intrusion into the polymer layer. The electric potential associated with that field satisfies Poisson's equation,

$$\frac{\partial^2 \psi}{\partial x^2}(x;t) = -\frac{\rho(x;t)}{4\pi\epsilon_r}, \quad 0 < x < D, \quad (26)$$

in the polymer layer, and the Poisson-Boltzmann equation,

$$\frac{\partial^2 \psi}{\partial x^2}(x;t) = -\frac{4\pi}{\epsilon_r} \sum_{i=1}^n z_i e n_i^\infty \exp(-ez_i \psi(x;t)/kT), \quad x > D, \quad (27)$$

external to the polymer layer. Here,  $n_i^\infty$  refers to the bulk ion density of mobile ion species  $i$ ,  $k$  is Boltzmann's constant,  $\epsilon_r$  is the relative dielectric permittivity of the matrix region and  $T$  is temperature in degrees Kelvin. The two solutions are complemented by the boundary conditions of, firstly, zero surface charge at  $x = 0$

$$\frac{\partial \psi}{\partial x}(x;t) = 0, \quad \text{at } x = 0, \quad (28)$$

secondly, the electroneutrality condition at infinity,

$$\frac{\partial \psi}{\partial x}(x;t) \rightarrow 0, \quad \text{as } x \rightarrow \infty, \quad (29)$$

and, finally, the conditions of continuity of electric potential and electric displacement at  $x = D$ , the interface between the polymer matrix and the electrolyte,

$$\begin{cases} \psi(D^-;t) = \psi(D^+;t), \\ \frac{\partial \psi}{\partial x}(D^-;t) = \frac{\partial \psi}{\partial x}(D^+;t), \end{cases} \quad (30)$$

where, in the last equation, we have assumed that the matrix and bulk electrolyte have the same relative dielectric permittivity.

Although the equations for the electric potential depend explicitly only on the spatial variable,  $x$ , the potential itself is also implicitly dependent on time,  $t$ , through its dependence on the charge density which depends explicitly and implicitly on time. Consequently, Poisson's equation



and the Poisson-Boltzmann equation need to be solved self-consistently throughout the time period of interest. Incidentally, the application of the Poisson-Boltzmann equation in the bulk solution implies the assumption of rapid equilibrium in the bulk. That is, irrespective of the time development within the polymer matrix, the electrolyte in the adjacent electrical double layer is taken to relax sufficiently fast to always be in a state of (quasi-)equilibrium given the prevailing conditions within the matrix.

### 3.5 Numerical solution approach

To solve the coupled systems of equations we first nondimensionalise all variables and equations using the time and spatial scales of  $D_m \kappa^2$  and  $\kappa^{-1}$ , respectively, where

$$C_m = \frac{\max_i \{n_i^\infty\}_1^n}{N_A 10^{-3}}, \quad D_m = \max_i \{D_i\}$$

$$\text{and } \kappa^2 = \frac{4\pi e^2}{\epsilon_r kT} \sum_{i=1}^n z_i^2 n_i^\infty. \quad (31)$$

We then introduce dimensionless dependent and independent variables and related parameters:  $y = \kappa x$ ,  $s = t D_m \kappa^2$ ,  $K = \kappa D$

$$D_i^* = \frac{D_i}{D_m}, \quad \phi = \frac{e\psi}{kT}, \quad C_X = \frac{[X]}{C_m}, \quad \mu_j^\pm = \frac{k_j^\pm C_m}{D_m \kappa^2}$$

$$\text{and } F_i = \frac{\Lambda_i^\infty kT}{N_A 10^{-3} e^2 D_m |Z_i|} \frac{Z_i}{|Z_i|}, \quad (32)$$

where  $\Lambda_i^\infty = N_A 10^{-3} e^2 |Z_i| / \lambda_i$  is the limiting ion conductance of species  $i$  while  $\lambda_i$  is the ionic drag coefficient for that ion.

The equations to be solved are then written in dimensionless form. For example, non-dimensional versions of the diffusion equations take the form

$$\frac{\partial C_j}{\partial s} = D_j^* \frac{\partial^2 C_j}{\partial y^2} - F_j \frac{\partial}{\partial y} \left[ C_j \frac{\partial \phi}{\partial y} \right] - \frac{\partial C_{jPEI}}{\partial s}$$

$$j = \{Cu, Zn\}, \quad 0 < y < K, \quad s > 0, \quad (33)$$

with a similar equation for  $Cl^-$ , but without the last term on the right hand side. The Poisson equation becomes

$$\frac{\partial^2 \phi}{\partial y^2} = -f(y; s) \equiv -\frac{1}{\sum_{i=1}^n z_i^2 C_i^\infty} \sum_{l=1}^{n+m} z_l C_l(y; s), \quad 0 < y < K, \quad (34)$$

Finally, the reaction equations (e.g., eq 2 and 3) typically appear in the form

$$\frac{\partial C_{jPEI}}{\partial s} = \mu_j^+ C_j C_{PEI} - \mu_j^- C_{jPEI} + \mu_3^+ C_j C_{IPEI} - \mu_3^- C_l C_{jPEI},$$

$$j \neq l = \{Cu, Zn\}, \quad s > 0. \quad (35)$$

Note that some dimensionless reaction rate constants are not defined as per eq 32, depending on their original dimensions. Nevertheless, dimensionless reaction rates are implicit in all of our working. We point out that for convenience we refrain in the sequel from quoting the units of the different reaction rate constants. Instead, we document here that the units of  $k_1^+$ ,  $k_2^+$ ,  $k_3^+$ ,  $k_3^-$  (Scenario I and II),  $k_4^-$  and  $k_5^\pm$  are  $\text{cm}^3 \text{molec}^{-1} \text{sec}^{-1}$ , while the units of  $k_1^-$ ,  $k_2^-$  and  $k_4^+$  are  $\text{sec}^{-1}$ . The units of  $k_3^-$  (rapid dissociation version of Scenario II) are  $\text{cm}^6 \text{molec}^{-2} \text{sec}^{-1}$ .

It is possible in principle to consider all three sets of equations (dimensional or nondimensional versions) as subsystems of a larger system of partial differential equations (*pdes*) involving both time ( $t$  or  $s$ ) and space ( $x$  or  $y$ ) derivatives. Those equations not possessing explicit time (space) derivatives can be considered as *pdes* with zero time (space) derivative coefficients. The complete system could theoretically be solved as one self-consistent system. Unfortunately, this turns out to be problematic in practice. In this work, we have adopted an iterative approach whereby we cycle through the solution of each subsystem in turn, assuming that the dependent variables *not* being solved for explicitly are inhomogeneous inputs in that calculation. The outputs of each subsystem calculation are then used as inputs for the solution of the other subsystems. The entire cycle of calculation is iterated until we achieve self-consistent results for a given set of initial parameter conditions. The code developed was written in the Matlab<sup>®</sup> environment utilizing some of the inbuilt subroutines. The subsystem of reaction equations of the form eq 35 was solved using the function routine *ode45*, while the set of diffusion equations, eq 33, was solved using the solver *pdepe*. With regard to eq 34, this equation was integrated explicitly to give the result

$$\phi(y; s) = \int_0^y f(y'; s) (y' - y) dy' + \Phi_0 \quad (36)$$

with  $\Phi_0$  to be determined from satisfaction of the continuity conditions at  $y = K$ :

$$\begin{cases} \Phi_0 + \int_0^K f(y'; s) (y' - K) dy' = \phi(K^+; s), \\ \int_0^K f(y'; s) (y' - K) dy' = \frac{\partial \phi}{\partial y}(K^+; s) \end{cases} \quad (37)$$

In eq 37, the right hand side of the second of the continuity equations is the derivative of the Poisson-Boltzmann solution:

$$\frac{\partial \phi}{\partial y}(K^+; s) = \pm \sqrt{\frac{2}{\sum_{i=1}^n z_i^2 C_i^\infty}} \sqrt{\sum_{l=1}^n C_l^\infty (e^{-Z_l \phi(K^+; s)} - 1)}, \quad (38)$$

which explicitly involves the solution evaluated at  $y = K$ . Equation 38 and the first of eq 37 represent a single closed transcendental equation that can be solved, say iteratively, for

**Table 1** Summary of parameter values used in model simulations (unless otherwise stated).

Parameter	Value	Comment
n, m	3, 3/4	Scenario I/Scenario II
$[Cu^{2+}]^\infty, [Zn^{2+}]^\infty, [Cl^-]^\infty$	1.0 mM, 1.0 mM, 4.0 mM	
$n_{PEI_{tot}}$	$6.022 \times 10^{17} \text{ cm}^{-3} \equiv 1.0 \text{ mM}$	
$n_{PEI_{1,tot}}$	$3.011 \times 10^{17} \text{ cm}^{-3} \equiv 0.5 \text{ mM}$	
$n_{PEI_{2,tot}}$	$3.011 \times 10^{17} \text{ cm}^{-3} \equiv 0.5 \text{ mM}$	
$Z_{PEI} = Z_{PEI_1} = Z_{PEI_2}$	-1	
$R_{Cu}$	1.074 Å	Unless otherwise stated
$R_{Zn}$	1.069 Å	
$R_{Cl}$	1.181 Å	
Polymer thickness, D	$10^{-6} \text{ cm}$	
$\Lambda_{Cu}^\infty$	$73.5 \text{ cm}^2 \text{ Ohm}^{-1}$	
$\Lambda_{Zn}^\infty$	$75 \text{ cm}^2 \text{ Ohm}^{-1}$	
$\Lambda_{Cl}^\infty$	$76.35 \text{ cm}^2 \text{ Ohm}^{-1}$	
Temperature, T	298 K	
$\epsilon_r$	78	For the bulk solution
$\epsilon_r$	78	Assumed for the polymer region

$\Phi_0$ . However, it turns out that for the charge conditions of interest here, the potential is sufficiently small in magnitude to justify invoking the linear Poisson-Boltzmann solution approximation outside of the polymer region. This greatly simplifies the procedure allowing  $\Phi_0$ , and thus the entire potential function within the matrix, to be determined explicitly. In this case we find that

$$\Phi_0 = \int_0^K f(y';s)(K-y')dy' + \int_0^K f(y';s)dy'. \quad (39)$$

## 4 Results and discussion

### 4.1 Scenario I

In this section we shall focus on Scenario I as an example of a system exhibiting the type of qualitative behavior found in the experiments of<sup>1</sup>. The working hypothesis of this scenario is that although both ions have a similar binding affinity for the PEI binding sites (or possibly that  $Cu^{2+}$  has a greater affinity for binding than  $Zn^{2+}$ ) the  $Zn^{2+}$  metal ion has a more rapid diffusive entry into the polymer matrix and therefore has an earlier binding association with the polymer than does  $Cu^{2+}$ . However, the hypothesis then proposes that once in, the  $Cu^{2+}$  ions preferentially replace already bound  $Zn^{2+}$  ions to either a significant fractional extent or completely, depending on the respective binding constants. Clearly, the important parameters to focus on in order to explore and test the hypothesis are the diffusion constants of the respective ions and the binding reaction rate constants introduced in the previous section. To this end (and so as to limit the very large parameter space inherent in the model) we focus attention on the principal parameters:  $k_{1,2}^\pm$ ,  $k_3^\pm$  and  $D_{1,2}$ , keeping other quantities constant.

Quantities such as the thickness of the polymer matrix,  $w$ , the bulk concentrations of free electrolyte ions,  $C_{Cu}^\infty$ ,  $C_{Zn}^\infty$ ,  $C_{Cl}^\infty$  and the density of binding sites serve only to adjust the total number of bound  $Cu^{2+}$  and  $Zn^{2+}$  ions (*i.e.*, the steady state) for a given set of our designated principal parameters. It is possible that under extreme parameter conditions, these secondary parameters may influence even the qualitative behavior. However, it will become clear that under quite reasonable parameter conditions, the model described in Section 3 does support the hypothesis. Table 1 summarizes the fixed parameters used in these calculations.

It has been shown<sup>30</sup> that the diffusion constants of the mobile electrolyte ions vary, depending on solution conditions. The ranges of diffusion constants,  $0.5 - 1.0 \times 10^{-5} \text{ cm}^2 \text{ s}^{-1}$  and  $2 - 5 \times 10^{-6} \text{ cm}^2 \text{ s}^{-1}$ , determined experimentally for  $Cu^{2+}$  and  $Zn^{2+}$  under concentrated electrolyte conditions are not too dissimilar to what can be deduced from the ideal Stokes-Einstein relation

$$D_{Einstein} = \frac{kT}{6\pi\eta R}, \quad (40)$$

assuming  $\eta$  is the viscosity of water and where  $R$  is the van der Waals radius of the ion. Taking van der Waals radii of 1.074 Å, 1.069 Å and 1.18 Å for  $Cu^{2+}$ ,  $Zn^{2+}$  and  $Cl^-$  gives the values of  $2.26 \times 10^{-6}$ ,  $2.27 \times 10^{-6}$  and  $2.06 \times 10^{-6} \text{ cm}^2 \text{ s}^{-1}$  for the ions' respective diffusion constants. As we have no knowledge yet of the effective diffusion constants of these ions in the polymer matrix, we shall utilize eq 40 to derive diffusion constants based on effective ion radii, in order to readily draw a comparison with diffusion in the bulk solution.

We first establish the reference case of ion binding assuming all-but equal diffusion constants and equal binding affinities. Under such conditions identical time and space develop-

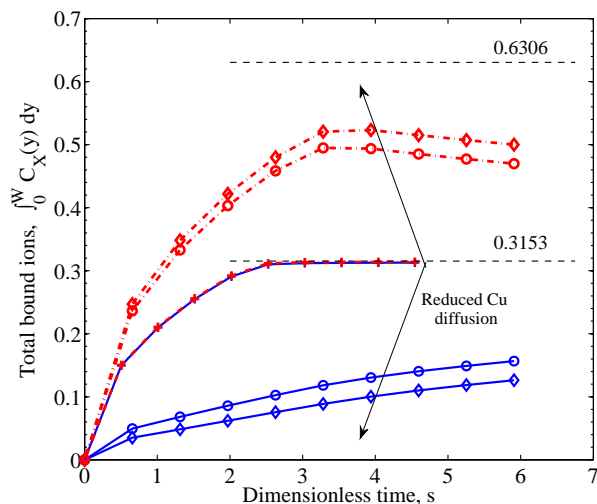


**Fig. 2** Integral graphs showing the rates of accumulation of CuPEI<sup>+</sup> and ZnPEI<sup>+</sup> assuming independent binding reactions. Blue solid lines denote CuPEI accumulation, while red broken lines depict ZnPEI<sup>+</sup> accumulation. Values shown are nondimensional. The thin black dashed lines indicate the level of saturated binding; the upper line denotes the level of saturated binding by one species, while the lower line indicates the level of equally shared saturated binding. The results were generated assuming direct binding rate constants of  $k_1^+ = k_2^+ = 5 \times 10^{11}$  and  $k_1^- = k_2^- = 4 \times 10^6$  and negligible exchange reaction,  $k_3^\pm = 1.0$ . In the order depicted by the arrows, we assume increasing effective Cu<sup>2+</sup> ion radius:  $R_{Cu} = 1.074$  (pluses), 3.5 (circles) and 4.5 (diamonds) Å, respectively, or equivalently decreasing Cu diffusion constant:  $D_{Cu} = 2.26 \times 10^{-6}$ ,  $6.94 \times 10^{-7}$  and  $5.40 \times 10^{-7}$  cm<sup>2</sup> s<sup>-1</sup>, respectively, compared with  $D_{Zn} = 2.27 \times 10^{-6}$  cm<sup>2</sup> s<sup>-1</sup>. Other parameters are as given in Table 1.

ment of the density of CuPEI<sup>+</sup> and ZnPEI<sup>+</sup> complexes within the polymer layer. One should note that steady state densities are obtained for all mobile ions well within the non-dimensional time frame adopted. The steady state concentrations of CuPEI<sup>+</sup> and ZnPEI<sup>+</sup> are dictated solely by the respective bulk ion concentrations and the underlying density of binding sites. The equivalence of the two ions results in negligible difference in either diffusive or absorptive behavior. This is summarized by the coincident curves in the centre of Figure 2. The figure shows the time evolution of the integral amounts of CuPEI<sup>+</sup> and ZnPEI<sup>+</sup> in the matrix. Mobile metal ions occupying space in the matrix are not included in these integral quantities. The curves have converged to the theoretical limit depicted by the dashed line, which represents the case of equal share of binding sites to Cu and Zn. The separated curves (blue solid curves for CuPEI<sup>+</sup> and red broken curves for ZnPEI<sup>+</sup>) on either side of the coincident pair de-

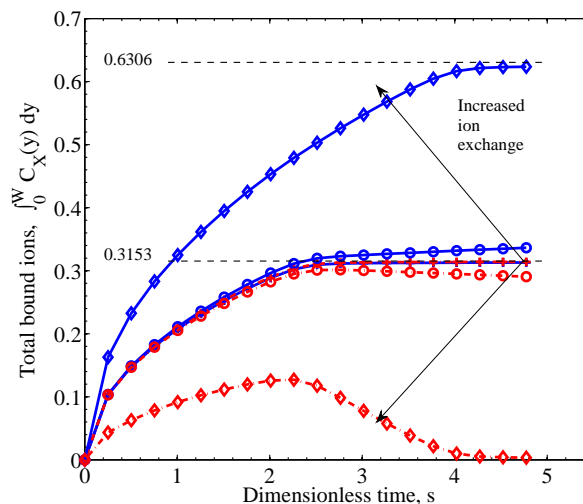


**Fig. 3** Integral graphs showing CuPEI<sup>+</sup> and ZnPEI<sup>+</sup> accumulation rates according to Scenario I. Line references as in Figure 2. This data was generated assuming equivalent direct binding rate constants:  $k_1^+ = k_2^+ = 5 \times 10^{11}$  and  $k_1^- = k_2^- = 4 \times 10^6$  and (practically) equivalent diffusion rates, while the different curves, in the order depicted by the arrows, result from increasing exchange reaction rate constants  $k_3^+ = 1.0$  (pluses),  $10^9$  (circles) and  $10^{12}$  (diamonds), respectively. Other parameters are as given in Table 1.

pic the result of delaying the influx of Cu<sup>2+</sup> by reducing this ion's diffusion constant. The two values of  $R_{Cu} = 3.5$  Å and 4.5 Å show progressively reduced Cu<sup>2+</sup> uptake with corresponding increased Zn<sup>2+</sup> uptake. The accumulating ZnPEI<sup>+</sup>, however, reaches a maximum and then decreases as CuPEI<sup>+</sup> continues to increase. However, the behavior is not due to any extraneous exchange process as negligible exchange has been assumed here ( $k_3^\pm = 1.0$ ). Instead what we observe is a natural approach of the two corresponding curves to their equal steady state values shown by the black dashed line in the figure centre. All things being equal, the differences in diffusive rates only affect the approach to equilibrium, not the equilibrium state itself. Thus, although we have not been able to track numerically the time development further, we surmise that the two sets of curves will each ultimately asymptote to the theoretical non-dimensional limit of 0.3153. (Numerical difficulties were experienced in solving the coupled system of diffusion equations, presumably because the faster species achieves steady state values in significant regions of the matrix before the overall system reached steady state. We aim to address this problem mathematically in future work.)

As our interest is with competitive absorption of metal ions over and above the intrinsic process depicted by the curves in Figure 2 and governed by eq 2 and 3, we show in Figure 3 the time development of total metal ions bound in the ma-

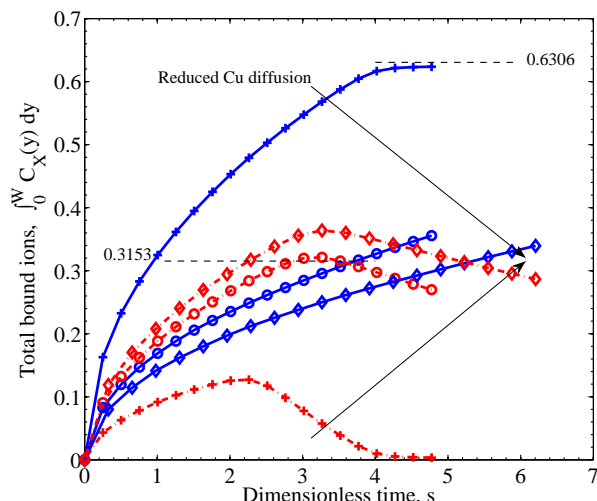


**Fig. 4** Integral graphs showing CuPEI<sup>+</sup> and ZnPEI<sup>+</sup> accumulation rates according to Scenario I. Line references as in Figure 2. The results were generated assuming: binding rate constants of  $k_1^+ = k_2^+ = 5 \times 10^{11}$  and  $k_1^- = k_2^- = 4 \times 10^6$ ; significant exchange reaction rate constants of  $k_3^+ = 10^{12}$   $k_3^- = 1.0$ . The different cases, in the order indicated by the arrows, refer to increasing effective Cu<sup>2+</sup> ion radius:  $R_{Cu} = 1.074$  (pluses), 4.5 (circles) and 6.5 (diamonds) Å, respectively, or equivalently decreasing Cu diffusion constant:  $D_{Cu} = 2.26 \times 10^{-6}$ ,  $5.40 \times 10^{-7}$  and  $3.74 \times 10^{-7}$  cm<sup>2</sup> s<sup>-1</sup>, respectively. All other parameters are as given in Table 1.

trix under equivalent diffusive and equal binding conditions, but with increasing influence of the forward exchange reaction. Three cases are demonstrated:  $k_3^+ = 1.0$ ,  $1.0 \times 10^9$  and  $1.0 \times 10^{12}$ . The blue solid curves again follow the accumulation of bound Cu<sup>2+</sup> throughout the polymer, while the red broken lines follow the accumulation of Zn<sup>2+</sup>. A nine order of magnitude increase in forward exchange reaction is required to see a separation of the integral responses. Initially, however, the two curves closely follow one another with the marginal diffusive advantage of Zn<sup>2+</sup> over Cu<sup>2+</sup> being insufficient to curtail the Cu<sup>2+</sup> binding dominance. At roughly twice the characteristic diffusion time, the two curves deviate markedly, with the CuPEI<sup>+</sup> integral curve increasing somewhat faster than linearly, while the ZnPEI<sup>+</sup> integral curve decreases linearly. The transition point is quite abrupt and common for the two curves. However, increasing  $k_3^+$  another three orders of magnitude results in complete separation of the two integral quantities, with the CuPEI<sup>+</sup> curve increasing monotonically with no apparent inflection point and plateau-ing to a steady state value (of 0.622), well above the maxima reached by the other two cases ( $k_3^+$  values) during the simulation period. In contrast, the ZnPEI<sup>+</sup> curve reaches a maximum at approximately twice the characteristic time before decreasing linearly

for another two characteristic time units to then asymptote to zero. The latter trend reflects the plateau-ing of CuPEI<sup>+</sup> at the high positive value. We point out that the plateau reached by the CuPEI<sup>+</sup> complex content asymptotes to the theoretical limit (0.6306) of all binding sites being occupied by the one species; this is indicated by the upper black dashed line. The implication here is that the added effect of an additional exchange process drives the system to consider Cu<sup>2+</sup> being the preferred binding species. Unfortunately again, we are unable to track the time course of metal ion accumulation in the case of the smaller value of  $k_3^+ = 10^9$  beyond the values shown. However, we anticipate that the two profiles for this case will ultimately asymptote to the same steady state limits as for the  $k_3^+ = 10^{12}$  profiles, namely zero for ZnPEI<sup>+</sup> and 0.6306 for CuPEI<sup>+</sup>.

The detailed time and space development of the concentrations of the metal ion-ligand complexes, CuPEI<sup>+</sup> and ZnPEI<sup>+</sup>, for the case of  $k_3^+ = 1.0 \times 10^{12}$  clearly exhibits the more rapid increase in ZnPEI<sup>+</sup> concentration initially. However, as Cu<sup>2+</sup> spreads into the matrix and the concentration of CuPEI<sup>+</sup> increases, the depletion of ZnPEI<sup>+</sup> in favorable exchange with CuPEI<sup>+</sup> is apparent (data not shown). The exchange effect is complete in the long term (*i.e.*, asymptotically) throughout the polymer matrix, but occurs sooner near to the edge of the polymer layer as this region is first to become saturated with Cu<sup>2+</sup> ions.

While we see a trend reflecting the differing degree of binding and specifically the replacement of bound Zn<sup>2+</sup> for bound Cu<sup>2+</sup> we have yet to encounter the observed event of initial dominant accumulation of Zn<sup>2+</sup> that is then overshadowed by the binding of Cu<sup>2+</sup>. If we now modify the diffusive process to disadvantage the diffusion of Cu by increasing the effective Cu<sup>2+</sup> radius to 4.5 Å, we find, other things being equal, the qualitative behavior observed in the experiments of Ref. <sup>1</sup>. In Figure 4, we compare the different cases of increased Cu<sup>2+</sup> radius  $R_{Cu} = 1.074$ , 4.5 and 6.5 Å, corresponding to a steady decrease in Cu<sup>2+</sup> diffusion constant. As in the case of Figure 2, the rate of intrusion of Cu<sup>2+</sup> is slower as  $R_{Cu}$  increases, allowing Zn to diffuse uninhibited into the matrix and bind with free PEI<sup>-</sup> sites. Only when a sufficient number of Cu<sup>2+</sup> ions have entered is there any decline in the rate of increase of bound Zn<sup>2+</sup>. However, in contrast to the results of Figure 2, the rate at which the metal ions bind is dominated by Zn<sup>2+</sup> only initially, when diffusion of Cu<sup>2+</sup> is much slower ( $R_{Cu} = 4.5$  Å compared with  $R_{Zn} = 1.069$  Å). A cross-over point is reached beyond which the rate of uptake of Cu<sup>2+</sup> dominates over Zn<sup>2+</sup> binding through the action of the exchange mechanism (eq 6). Increasing  $R_{Cu}$  to 6.5 Å reinforces the effect, although the peak value of ZnPEI<sup>+</sup> is only slightly higher and is reached at only a slightly later time ( $s = 3.32$  for  $R_{Cu} = 6.5$  Å compared with  $s = 3.19$  for  $R_{Cu} = 4.5$  Å). The cross-over point, however, is significantly delayed in the slower diffusive

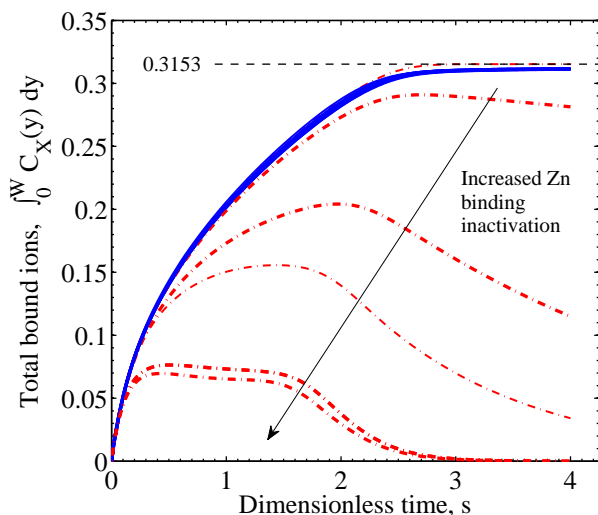


**Fig. 5** Integral graphs showing CuPEI<sup>+</sup> and ZnPEI<sup>+</sup> accumulation rates according to Scenario II with and without an intermediate dissociation step. Values shown are nondimensional. Blue solid lines denote CuPEI<sup>+</sup> accumulation, while red broken lines depict total ZnPEI<sup>+</sup> accumulation (in some cases being the sum of both ZnPEI<sub>2,a</sub><sup>+</sup> and ZnPEI<sub>2,ia</sub><sup>+</sup>). Values shown are nondimensional. The results were generated assuming equivalent binding rate constants  $k_1^+ = k_2^+ = 5 \times 10^{11}$  and  $k_1^- = k_2^- = 4 \times 10^6$  and equivalent ion diffusion rates. Thin lines correspond to the case of an intermediate dissociation reaction, while thick lines assume no intermediate reaction step. The thin black dashed line indicates the level of saturated binding for both site types. In the order depicted by the arrow, the ZnPEI<sup>+</sup> curves result from increased site inactivation reaction (eq 13 and eq 17):  $k_3^\pm = k_4^\pm = k_5^\pm = 1.0$ ;  $k_3^+ = 10^9$ ,  $k_3^- = 1.0$ ,  $k_5^\pm = 1.0$ ;  $k_3^+ = 10^{11}$ ,  $k_3^- = 1.0$ ,  $k_5^\pm = 1.0$ ;  $k_3^+ = 10^{12}$ ,  $k_3^- = 1.0$ ,  $k_4^+ = 10^7$ ,  $k_4^- = k_5^\pm = 1.0$ ;  $k_3^+ = 10^{11}$ ,  $k_3^- = 1.0$ ,  $k_5^+ = 10^9$ ,  $k_5^- = 1.0$ ;  $k_3^+ = 10^{11}$ ,  $k_3^- = 1.0$ ,  $k_5^+ = 10^{11}$ ,  $k_5^- = 1.0$ . All other parameters are as given in Table 1.

case ( $s = 5.26$  for  $R_{Cu} = 6.5$  Å compared with  $s = 3.22$  for  $R_{Cu} = 4.5$  Å). Although we are not able to access later simulation times in the cases of  $R_{Cu} = 4.5$  Å and  $R_{Cu} = 6.5$  Å due to numerical difficulties, we again anticipate that the subsequent behavior of the profiles will mimic the asymptotic behavior exhibited by the faster Cu<sup>2+</sup> diffusion case ( $R_{Cu} = 1.074$  Å), since once again the only difference between the cases (difference in the diffusion constant of Cu<sup>2+</sup>) only affects the rate of approach to steady state and not the steady state condition itself.

The combination of the observed short term behavior, depicted by the  $R_{Cu} = 4.5$  Å and  $R_{Cu} = 6.5$  Å results, with the expected asymptotic limit, demonstrated by the  $R_{Cu} = 1.074$  Å result, correlates well with the behavior observed in the Lindén, *et al.* experiments.

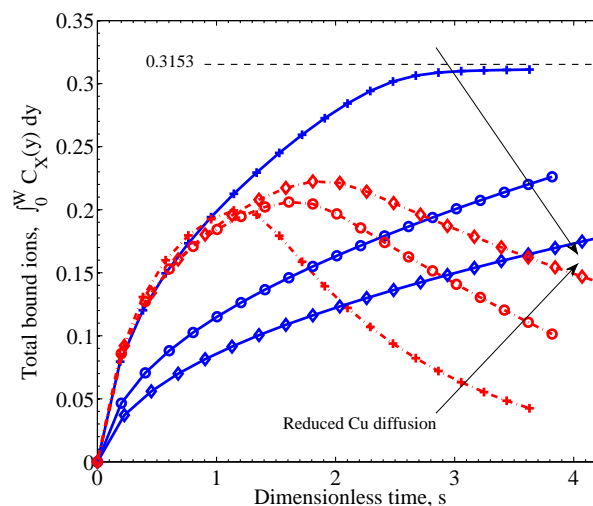


**Fig. 6** Integral graphs showing CuPEI<sup>+</sup> and ZnPEI<sup>+</sup> accumulation rates according to Scenario II with an intermediate dissociation step. Line references as in Figure 5. In the order depicted by the arrows, we assume increasing effective Cu radius:  $R_{Cu} = 1.074$  (pluses), 3.5 (circles) and 6.5 (diamonds) Å, respectively, or equivalently decreasing Cu diffusion constant:  $D_{Cu} = 2.26 \times 10^{-6}$ ,  $6.94 \times 10^{-7}$  and  $3.74 \times 10^{-7}$  cm<sup>2</sup> s<sup>-1</sup>. Reaction rate constants assumed are: equivalent binding rate constants  $k_1^+ = k_2^+ = 5 \times 10^{11}$  and  $k_1^- = k_2^- = 4 \times 10^6$ ; binding site inactivation  $k_3^+ = 10^{12}$ ,  $k_5^+ = 10^9$  and  $k_3^- = k_5^- = 1.0$ ; and intermediate step dissociation rate  $k_4^+ = 10^7$  and  $k_4^- = 1.0$ . All other parameters are as given in Table 1.

## 4.2 Scenario II

In the following calculations we shall assume the same total number density of absorption sites as assumed for Scenario I. This is to allow for some commonality between the two models. In the majority of cases, however, half of these are assumed selective binding sites for Cu<sup>2+</sup> and half are selective binding sites for Zn<sup>2+</sup>. Again in the majority of cases, the binding of metal ions will be limited only to their respective sites. As a point of model differentiation, this scenario models, more explicitly than in Scenario I, the situation of Cu<sup>2+</sup> binding having a direct impact on the binding of Zn<sup>2+</sup> through two mechanisms.

The first mechanism is akin to the mechanism underpinning Scenario I but rather than being considered an exchange process, the mechanism implies an induced conformational change to the polymer structure that destabilizes existing ZnPEI<sup>+</sup> complexes. A destabilized complex then undergoes a dissociation reaction to produce a free Zn<sup>2+</sup> ion and an inactive PEI<sub>2,ia</sub><sup>-</sup> binding site. The second mechanism is not considered at all in Scenario I. Here, the binding of Cu<sup>2+</sup> impacts directly on a bare PEI<sub>2,a</sub><sup>-</sup> binding site, converting it to its inac-



tive state thus precluding any subsequent  $\text{Zn}^{2+}$  binding. With regard to the former mechanism, we treat it here in two ways. First, by modelling explicitly the dissociation process as a separate, but coupled, reaction step, with its own dissociation rate constants ( $k_4^\pm$  in eq 14); as already mentioned a nonzero  $k_4^-$  constant allows for the finite probability of a reverse reaction, however slight. Nevertheless, we choose  $k_4^-$  values that have negligible effect on the simulation outcome. In the second approach, we assume that the forward dissociation reaction proceeds spontaneously and completely without the possibility of reversal. The two cases are clearly distinguished in the figures. In this case, there is no reference to  $k_4^\pm$  constants and we invoke eq 15 (again with negligible  $k_3^-$  values). For the right choice of reaction rate constants, the second approach is largely equivalent to the first although it circumvents the need to identify possible  $k_4^\pm$  values.

In Figure 5 we demonstrate the effect of increasing the effect of polymer reconfiguration triggered by the binding of  $\text{Cu}^{2+}$  ions, manifested in the destabilisation of existing  $\text{ZnPEI}_{2,a}^+$  complexes and the inactivation of bare  $\text{PEI}_{2,a}^-$  sites. In this figure both treatments of the two-site model, with and without an intermediate dissociation step, are included to indicate their essential equivalence. Two points should be noted. First, with the separation into two site types, the theoretical limit of site saturation is equal for the each binding species. This is indicated by the black dashed line and value of 0.3153. However, in contrast to Scenario I, as the binding of  $\text{Zn}^{2+}$  decreases through the destabilisation mechanisms there is no corresponding increase in the level of  $\text{Cu}^{2+}$  binding. Hence, in all the cases shown in this figure, the  $\text{CuPEI}_1^+$  integral curve is largely unaffected by the changes experienced by the  $\text{ZnPEI}_{2,a}^+$  content in the matrix. The second point of note is that the curves were generated assuming equivalent ion diffusive rates (equal diffusion constants). Note also the absence of the experimentally observed behavior of initial dominance of bound  $\text{Zn}^{2+}$  over bound  $\text{Cu}^{2+}$  and subsequent reversal of binding trends. This sought-after behavior, quite convincingly demonstrated in Figure 6, is found when differences in diffusivities are introduced. Specifically, as the rate of  $\text{Cu}^{2+}$  intrusion into the matrix is successively reduced (by reducing the ion's diffusion constant relative to that of  $\text{Zn}^{2+}$ ) there is a progressively stronger take up of  $\text{Zn}^{2+}$ , at least in relative terms. However, the uptake of  $\text{Zn}^{2+}$  never exceeds the theoretical limit (of 0.3153) and indeed it is always lower and slower than the amount taken up in the case of completely independent binding, which thus represents an upper limiting envelope in time for  $\text{Zn}^{2+}$  uptake. This observation is to be contrasted with the results of Scenario I in which the  $\text{ZnPEI}^+$  amounts can surpass the equal binding curve. Naturally, as the  $\text{Cu}^{2+}$  diffusion constant is reduced, the  $\text{ZnPEI}_{2,a}^+$  accumulation is larger, lying closer to the independent binding envelope. In all cases of  $\text{Cu}^{2+}$  diffusion, however, the  $\text{ZnPEI}_{2,a}^+$  curve attains a maxi-

mum after which the level of bound  $\text{Zn}^{2+}$  decreases linearly (at first) before approaching the zero asymptote in the steady state limit, as more  $\text{Cu}^{2+}$  binds to its specific binding site. The results in this figure were generated assuming an intermediate dissociation step.

It should be noted that as we have assumed an equal number of binding sites for  $\text{Cu}^{2+}$  as for  $\text{Zn}^{2+}$ , the steady state limit for the amount of  $\text{ZnPEI}_{2,a}^+$  complexes will be zero. This limit would apply for any choice of underlying site densities satisfying the inequality  $n_{\text{PEI}_{1,\text{tot}}} \geq n_{\text{PEI}_{2,\text{tot}}}$ . However, a nonzero steady state  $\text{ZnPEI}_{2,a}^+$  limit exists under the current binding scenario should the underlying  $\text{Cu}^{2+}$  binding site density  $n_{\text{PEI}_{1,\text{tot}}}$  be less than  $n_{\text{PEI}_{2,\text{tot}}}$ . Since experimental findings indicate complete depletion of bound  $\text{Zn}^{2+}$ , this would suggest that the number of  $\text{Cu}^{2+}$  binding sites to be greater than or equal to the number of  $\text{Zn}^{2+}$  binding sites.

Figure 7A shows the time and space development of the  $\text{ZnPEI}_{2,a}^+$  complex under the condition of reduced  $\text{Cu}^{2+}$  diffusion and significant rates of inactivation and destabilisation. In B we show the corresponding increase in the density of inactive  $\text{Zn}^{2+}$  binding sites,  $\text{PEI}_{2,ia}^-$ . The latter quantity appears in response to the level of influx of  $\text{Cu}^{2+}$  and thus the time and space dependent  $\text{CuPEI}_1^+$  density.

For completeness, we show in Figure 8 results of the model assuming no intermediate dissociation step in Scenario II, again for significant inactivation and destabilisation reactions and for progressively reduced  $\text{Cu}^{2+}$  diffusion. No major qualitative differences appear in comparison with the results shown in Figure 6.

## 5 Summary remarks

With regard to Scenario I, we have shown that with the right combination of two influential factors,

- a low relative  $\text{Cu}^{2+}$  diffusion constant,
- a high  $\text{Cu}^{2+}$  for  $\text{Zn}^{2+}$  exchange rate,

that we can reproduce qualitatively, if not quantitatively, the experimental findings of<sup>1</sup>. Naturally, it is necessary for the  $\text{Cu}^{2+}$  binding rate/strength to be sufficiently high for the  $\text{Cu}^{2+}$  binding to be at all competitive with  $\text{Zn}^{2+}$ . However, the results indicate that it is not necessary for  $\text{Cu}^{2+}$  binding to be significantly stronger than the binding strength of  $\text{Zn}^{2+}$ . The combination of the above two factors is sufficient to substantiate the hypothesis of a simple competitive mechanism (or mechanisms) for the reported experimental results. We remark that this scenario is the simpler of the two presented here. Advocates of Occam's razor would argue that this may be the most reasonable explanation. We remark also that nothing has actually been said of, nor does the model itself suggest, any

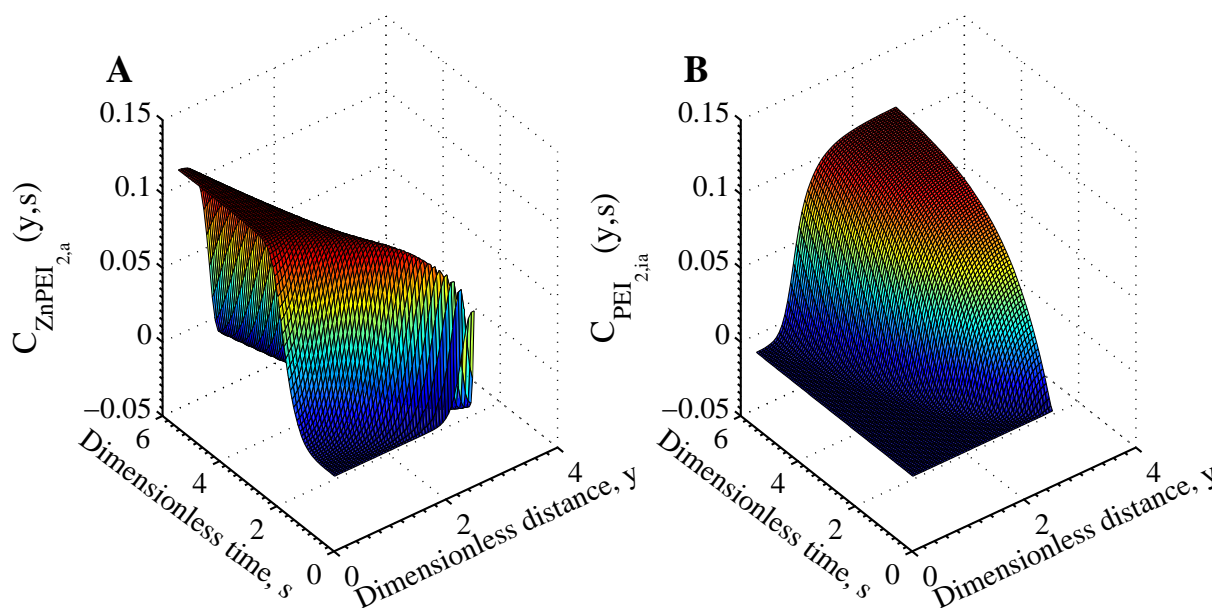


**Fig. 7** Surface plots showing the temporal and spatial increase of bound species and inactivated Zn binding sites according to Scenario II with an intermediate dissociation step. The results assume the conditions of Figure 6 for the extreme case of reduced  $\text{Cu}^{2+}$  diffusion rate ( $D_{\text{Cu}} = 3.74 \times 10^{-7} \text{ cm}^2 \text{ s}^{-1}$  compared with  $D_{\text{Zn}} = 2.27 \times 10^{-6} \text{ cm}^2 \text{ s}^{-1}$ ). The subplots show (A)  $\text{ZnPEI}_{2,ia}^+$  density and (B)  $\text{PEI}_{2,ia}^-$  density. All variables are nondimensional.

specific physical or chemical processes that are being represented by the rate constants themselves.

With regard to Scenario II, analogous summary comments can be made. A diffusion differential alone is not sufficient to explain the experimental findings. Nor is a polymer matrix rearrangement triggered by  $\text{Cu}^{2+}$  binding sufficient to account for the observed competitive binding behavior. The qualitative effect can be achieved through a suitable blend of these two mechanisms:

- significant differential diffusion, and
- significant destabilization of  $\text{Zn}^{2+}$ - $\text{PEI}^-$  complexes and/or inactivation of  $\text{Zn}^{2+}$  binding sites

Incidentally, this is true whether  $\text{Cu}^{2+}$  and  $\text{Zn}^{2+}$  have different selective binding sites or they are attracted to and compete for the same binding sites (data not shown).

The features that distinguish the single site model from the two site model are points of differentiation that are potentially useful in aiding the interpretation of experiments on the real systems as well as for the design of new experiments for hypothesis testing.

In this work we have not made any attempt to accurately model the experimental system. Instead, we have taken the opportunity to explore the temporal and spatial details that

physically underlie the competitive binding process. We have achieved the goal of identifying the essential processes that lead to preferential competitive binding. In our ongoing efforts, which will be the subject of future communications, we are undertaking the necessary rigorous quantitative comparison between theory and a more extensively characterized experimental system. In so doing the model will be refined to improve its representation of the experimental system. This will include a more appropriate spatial account of ion diffusion through the porous matrix<sup>29</sup> and allowing for the possibility of matrix swelling during the absorption process. More accurate modelling, however, requires in turn a more accurate characterisation of the experimental situation as well as a more extensive survey of experimental conditions. Not only will this establish a solid benchmark of experimental data for a comparison, it will help to identify trademark behavior that could be used to distinguish between the different possible mechanisms responsible for the observed competitive ion absorption.

**Acknowledgements.** The authors thank Dr. Mikael Larsson for useful discussions. We also thank Drs Hamid Laga and Pankaj Kumar and Ms Julie Sleep for technical assistance with Matlab programming and Latex formatting, respectively.

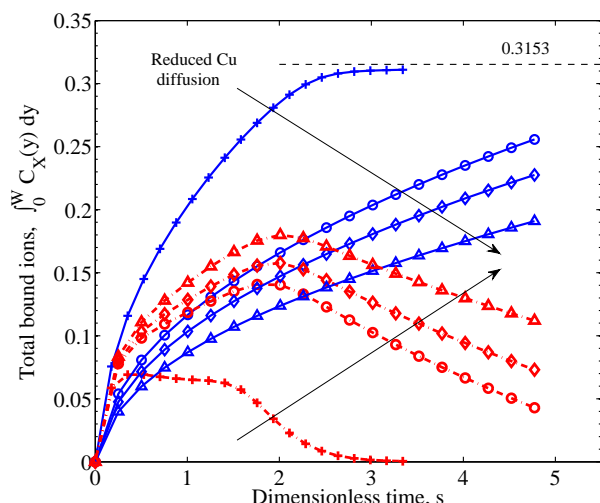


**Fig. 8** Integral graphs showing CuPEI<sup>+</sup> and ZnPEI<sup>+</sup> accumulation rates according to Scenario II with no intermediate dissociation step. Line references as in Figure 5. In the order depicted by the arrows, we assume increasing effective Cu radius:  $R_{Cu} = 1.074$  (pluses), 3.5 (circles), 4.5 (diamonds) and 6.5 (triangles) Å, respectively, or equivalently decreasing Cu diffusion constant:  $D_{Cu} = 2.26 \times 10^{-6}$ ,  $6.94 \times 10^{-7}$ ,  $5.40 \times 10^{-7}$  and  $3.74 \times 10^{-7}$  cm<sup>2</sup> s<sup>-1</sup>. We assume the following rate constants: equivalent binding rate constants  $k_1^+ = k_2^+ = 5 \times 10^{11}$  and  $k_1^- = k_2^- = 4 \times 10^6$ ; inactivation rates of  $k_3^+ = 10^{11}$ ,  $k_5^+ = 10^{11}$  and  $k_3^- = k_5^- = 1.0$ . All other parameters are as given in Table 1.

## References

- Lindén, J. B.; Larsson, M.; Coad, B. R.; Skinner, W. M.; Nydén, M. Polyethyleneimine for Copper Absorption: Kinetics, Selectivity and Efficiency in Artificial Seawater. *R. S. C. Advances*, **2014**, *4*, 25063-25066.
- Beatty, S. T.; Fischer, R. J.; Hagers, D. L.; Rosenberg, E. A Comparative Study of the Removal of Heavy Metal Ions from Water Using a Silica-Polyamine Composite and a Polystyrene Chelator Resin. *Indust. Eng. Chem. Res.*, **1999**, *38*, 4402-4408.
- Kiaune, L.; Singhasemanon, N. Pesticidal Copper (I) Oxide: Environmental Fate and Aquatic Toxicity. *Rev Environ Contamin. Toxicology*, **2011**, *213*, 1-26.
- Schiff, K.; Diehl, D.; Valkirs, A. Copper Emissions from Antifouling Paint on Recreational Vessels. *Marine Poll. Bull.*, **2004**, *48*, 371-377.
- Duru, P. E.; Bektas, S.; Genc, Ö.; Patir, S.; Denizli, A. Adsorption of Heavy-Metal Ions on Poly(Ethyleneimine)-Immobilized Poly(Methyl Methacrylate) Microspheres. *J. Applied Poly. Sci.*, **2001**, *81*, 197-205.
- Fu, F.; Wang, Q. Removal of Heavy Metal Ions from Wastewaters: A Review. *J. Environ. Managem.*, **2011**, *92*, 407-418.
- Alexandratos, S. D. Ion-Exchange Resins: A Retrospective from Industrial and Engineering Chemistry Research. *Indust. Eng. Chem. Res.*, **1999**, *48*, 388-398.
- Chouyyok, W.; Shin, Y.; Davidson, J.; Samuels, W. D.; LaFemina, N. H.; Rutledge, R. D.; Fryxell, G. E.; Sangvanich, T.; Yantasee, W. Selective Removal of Copper(II) from Natural Waters by Nanoporous Sorbents Functionalized with Chelating Diamines. *Environ. Sci. Tech.*, **2010**, *44*, 6390-6395.
- Wan Ngah, W. S.; Kamari, A.; Koay, Y. J. Equilibrium and Kinetics Studies of Adsorption of Copper (II) on Chitosan and Chitosan/PVA Beads. *Int. J. Biol. Macromol.*, **2004**, *34*, 155-161.
- Foo, K. Y.; Hameed, B. H. Insights into the Modeling of Adsorption Isotherm Systems. *Chem. Eng. J. (Lausanne)*, **2010**, *156*, 2-10.
- Webster, A.; Halling, M. D.; Grant, D. M. Metal Complexation of Chitosan and its Glutaraldehyde Cross-Linked Derivatives. *Carbohydrate Res.*, **2007**, *342*, 1189-1201.
- Debbaudt, A.; Zalba, M.; Ferreira, M. L.; Gschaidner, M. E. Theoretical and Experimental Study of Pb<sup>2+</sup> and Hg<sup>2+</sup> Adsorption on Biopolymers. 2. Experimental Part. *Macromol. Biosci.*, **2001**, *1*, 6249-6257.
- Nurchi, V. M.; Crisponi, G.; Crespo-Alonso, M.; Lachowicz, J. I.; Szewczuk, Z.; Cooper, G. J. S. Complex Formation Equilibria of Cu<sup>II</sup> and Zn<sup>II</sup> with Triethylenetetramine and its Mono- and Di-acetyl Metabolites. *Dalton Trans.*, **2013**, *42*, 6161-6170.
- Hirata, S.; Ishida, Y.; Aihara, M.; Honda, K.; Shikino, O. Determination of Trace Metals in Seawater by On-line Column Preconcentration Inductively Coupled Plasma Mass Spectrometry. *Analytica Chimica Acta*, **2001**, *438*, 205-214.
- Lagerström, M. E.; Field, M. P.; Séguret, M.; Fischer, L.; Hann, S.; Sherrell, R. M. Automated On-line Flow-Injection ICP-MS Determination of Trace Metals (Mn, Fe, Co, Ni, Cu and Zn) in Open Ocean Seawater: Application to the GEOTRACES Program. *Marine Chem.*, **2013**, *155*, 71-80.
- Chen, Y.; Pan, B.; Li, H.; Zhang, W.; Lv, L.; Wu, J. Selective Removal of Cu(II) Ions by Using Cation-exchange Resin-Supported Polyethyleneimine (PEI) Nanoclusters. *Environ. Sci. Tech.*, **2010**, *44*, 3508-3513.
- Ghoul, M.; Bacquet, M.; Morcellet, M. Uptake of Heavy Metals from Synthetic Aqueous Solutions using Modified PEI-Silica Gels. *Water Res.*, **2003**, *37*, 729-734.
- Gao, B.; An, F.; Liu, K. Studies on Chelating Adsorption Properties of Novel Composite Material Polyethyleneimine/Silica Gel for Heavy-Metal Ions. *Appl. Surf. Sci.*, **2003**, *256*, 1946-1952.

- 19 Kobayashi, S.; Hiroishi, K.; Tokunoh, M.; Saegusa, T. Chelating Properties of Linear and Branched Poly(ethylenimines). *Macromolecules*, **1987**, *20*, 1496-1500.
- 20 Rivas, B. L.; Geckeler, K. E. *Polymer Synthesis Oxidation Processes*. Springer, **1992**.
- 21 Kislenko, V. N.; Oliynyk, L. P. Complex Formation of Polyethyleneimine with Copper(II), Nickel(II), and Cobalt(II) Ions. *J. Polym. Sci. Part A: Poly. Chem.*, **2002**, *40*, 914-922.
- 22 Yeagle, P. L. *The Structure of Biological Membranes, 2nd Ed.*. CRC Press, **2004**.
- 23 Miklavic, S. J.; Ninham, B. W. Conformation of Surface Bound Polyelectrolytes: I Implications for Cell Electrophoresis. *J. Theor. Biol.*, **1989**, *137*, 71-89.
- 24 Granfeldt, M. K.; Miklavic, S. J.; Marcelja, S.; Woodward, C. E. Conformation of Surface Bound Polyelectrolytes: II A Monte Carlo study of Medium Length Lattice Chains. *Macromolecules*, **1990**, *23*, 4760-4768.
- 25 Verwey, E. J. W.; Overbeek, J. Th. G. *Theory of the Stability of Lyophobic Colloids*. Elsevier Publishing Company, **1948**.
- 26 Evans, D. F.; Wennerström, H. *The Colloidal Domain*. VCH, New York, **1994**.
- 27 Attard, P. A. and Miklavic, S. J. The Electrical Double Layer in the Wall-Wall Hypernetted Chain Approximation with Bridge Functions. *J. Chem. Phys.*, **1993**, *99*, 6078-6086.
- 28 Miklavic, S. J.; Ninham, B. W. Competition for Adsorption Sites by Hydrated Ions. *J. Coll. Int. Sci.*, **1990**, *134*, 305-311.
- 29 Kim, J. T.; Anderson, J. L. Diffusion and Flow Through Polymer-Lined Micropores. *I & E. C. Research*, **1991**, *29*, 1008-1016.
- 30 Kariuki, S.; Dewald, H. D. Evaluation of Diffusion Coefficients of Metallic Ions in Aqueous Solutions. *Electroanalysis*, **1996**, *8*, 307-313.